Detection and Modelling of Nonlinear Elastic Response in Damaged Composite Structures

F. Ciampa[1], E. Onder[1], E. Barbieri[2], M. Meo[1*]

[1]*Material Research Centre, Department of Mechanical Engineering, University of Bath, Bath, BA2 7AY, UK*

[2]*The School of Engineering and Material Science, Queen Mary, University of London, Mile End Road, London, E1 4NS, UK*

*Corresponding author: m.meo@bath.ac.uk

Abstract

In this paper the nonlinear material response of damaged composite structures under periodic excitation is experimentally and numerically investigated. In particular, the nonlinear wave propagation problem was numerically analysed through a finite element model able to predict the nonlinear interaction of acoustic/ultrasonic waves with damage precursors and micro-cracks. Such a constitutive model is based on the Landau's semi-analytical approach to account for anharmonic effects of the medium, and is able to provide an understanding of nonlinear elastic phenomena such as the second harmonic generation. Moreover, Kelvin tensorial formulation was used to extend the wave propagation problem in orthotropic materials to the 3D Cartesian space. In this manner, the interaction of the stress waves with the 3D crack could be analysed. This numerical model was then experimentally validated on a composite plate undergone to impact loading. Good agreement between the experimental and numerical second

harmonic response was found, showing that this material model can be used as a simple and useful tool for future structural diagnostic applications.

Keywords: Nondestructive Evaluation Techniques, Nonlinear Ultrasound, Finite Element Method, Multiscale Modelling.

1 Introduction

Composite materials are renowned for their high strength to weight ratio, resistance to fatigue and low thermal expansion. However, due to their fragility to foreign object impacts, they present challenges for damage detection as much of the flaw is often interlaminar and not readily detectable. Such a defect is commonly referred to barely visible impact damage (BVID) and, if not promptly identified, it may cause strength and stiffness reductions driving the structure to collapse.

In the last few decades, a number of acoustic/ultrasonic-based Non-destructive (NDT) Evaluation techniques and Structural Health Monitoring (SHM) systems were developed to provide an early detection and warning of critical defects [1], [2]. Most of them analyse the variations of linear properties of the elastic waves propagating into the medium due to the presence of damage. Indeed, changes of the wave speed and amplitude can be used as a signature to access the location and severity of structural anomalies. However, acoustic/ultrasonic methods based on classical linear elastodynamic theory can be difficult to apply to inhomogeneous materials, such as composite laminates, and, in general, to damaged structures where the crack size is comparable with the wavelength (e.g. micro-cracks, delamination, inclusions, etc…) [3].

Recent studies have shown that nonlinear ultrasonic measurements are sensitive to low levels of defects and they can be used for detecting damages at their earliest stages [4], [5]. In particular, it was analytically and experimentally shown that the progressive degradation of the material structure and the presence of cracks create ultrasonic wave distortion along the wave propagation path. From a physical point of view, when a damage specimen is excited by an external dynamic load, the excitation produces compressive and tensile stresses on the edges of the crack, causing its "clapping" motion [6]. Hence, due to mechanical contacts between the crack interfaces, the wave induced response of the material generates nonlinear elastic effects such as higher harmonics of the excitation frequency [7].

Therefore, nonlinear elastic wave spectroscopy (NEWS) and phase symmetry analysis (PSA) techniques were developed to provide an effective means to characterise the structural damage by investigating the magnitude of higher (even) harmonics caused by nonlinear material behaviour [8], [9]. Particularly, as the second harmonic is quadratic with the amplitude of the fundamental frequency, it can be used as a signature of the presence of cracks or delamination within the medium [10]. Simplified nonlinear elastic theories have attempted to significantly provide an understanding of the generation of nonlinear phenomena in metallic and composite structures, especially in the presence of micro-cracks [11], [12], [13], [14]. However, these analytical approaches are mainly 1D or 2D and they may not succeed in reproducing the whole set of observed phenomena. Hence, numerical models can be used as an alternative for a more complete analysis, including the extension to the 3D space for anisotropic structures [15], [16], [17], [18].

The aim of this paper is to experimentally and numerically investigate nonlinear material responses of damaged composite structures. In particular, the nonlinear wave propagation problem was numerically analysed through a nonlinear elastic material model for the simulation of the acoustic/ultrasound stress waves with micro-cracks. Such a constitutive model is implemented in an explicit in-house finite element (FE) numerical software and it is based on the Landau's semi-analytical approach to account for anharmonic effects of the medium. In particular, the nonlinear structural response of the damaged material under continuous periodic (harmonic) input is represented through a finite number of FE elements with varying properties defining their nonlinear stress-strain relationship. Moreover, Kelvin tensorial formulation was used to extend the wave propagation problem in orthotropic materials to the 3D Cartesian space. In this manner, the interaction of the stress waves with the 3D crack could be analysed. As a result, it was possible to numerically reproduce nonlinear experimentally-observed phenomena such as the even (second) harmonic generation effect. This numerical model was then experimentally validated on a composite plate undergone to impact loading. Good agreement between the experimental and numerical second harmonic response was found, showing that this material model is able to provide an understanding of nonlinear elastic phenomena in composite structures with different levels of damages.

The layout of the paper is as follows: in Section 2 the 3D nonlinear elastic model for composite structures is presented. Section 3 reports the numerical test case used for the comparison with experimental test, whilst Section 4 illustrates the experimental set-up and the NDT techniques (C-scan and CT-scan) used to detect and access the damaged area. The comparison between the numerical and experimental results is presented in Section 5 and then, the conclusions of the paper are discussed.

2 Nonlinear Constitutive Model

Linear stress-strain relationship defined in Hooke's law is usually inadequate to describe the nonlinear mechanical behaviour of solids with distributed damage (micro-cracks and micro voids) and with inelastic behaviour [19], [20]. Indeed, damaged materials such as aluminium, steel and composites that have atomic elasticity arising from atomic-level forces between atoms and molecules, exhibit classical nonlinear (also known as *anharmonic*) effects which can be described by the nonlinear elastic theory of Landau [21]. Particularly, the expression of the nonlinear elastic modulus K_C can be obtained through a 1D power law expansion of the stress with respect to the strain ε:

$$K_C = K_0\left(1 + \beta\varepsilon + \delta\varepsilon^2 + \cdots\right) \tag{1}$$

where K_0 is the linear elastic modulus, β and δ are classical second order and third order nonlinear coefficients. However, for most of solids only the first nonlinear term β can be sufficient to predict the material's nonlinear response. This coefficient can be experimentally obtained from the measurement of the second harmonic amplitude generated from a single pure tone input [22]. Moreover, since Eq. (1) represents a scalar model, it cannot be used to investigate the 3D anisotropic material behaviour of a cracked sample to different types of waves (bulk waves, guided waves, etc…) (Fig. 1).

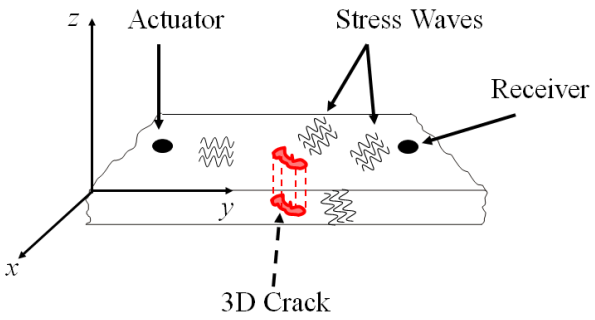

Figure 1 Material nonlinear response with a 3D crack.

Hence, to overcome this limitation, Kelvin notation was used to extend the standard Voigt stress-strain formulation in a tensorial equivalent form for the 3D Cartesian space [23]. Indeed, by introducing Kelvin representation, the Voigt stress-strain relationship for a homogeneous orthotropic elastic medium becomes:

$$\tilde{\boldsymbol{\sigma}} = \tilde{\mathbf{K}}\tilde{\boldsymbol{\varepsilon}} \tag{2}$$

where the new components of the 6D stress and strain vectors are:

$$\begin{aligned} \tilde{\boldsymbol{\sigma}} &= \left(\sigma_{11}, \sigma_{22}, \sigma_{33}, \sqrt{2}\sigma_{12}, \sqrt{2}\sigma_{13}, \sqrt{2}\sigma_{23}\right)^T \\ \tilde{\boldsymbol{\varepsilon}} &= \left(\varepsilon_{11}, \varepsilon_{22}, \varepsilon_{33}, \sqrt{2}\varepsilon_{12}, \sqrt{2}\varepsilon_{13}, \sqrt{2}\varepsilon_{23}\right)^T \end{aligned} \tag{3}$$

and $\tilde{\mathbf{K}}$ is the new six by six stiffness matrix defined by:

$$\tilde{\mathbf{K}} = \mathbf{TKT} \text{ with } \mathbf{T} = \begin{bmatrix} \mathbf{I} & 0 \\ 0 & \sqrt{2}\mathbf{I} \end{bmatrix} \tag{4}$$

where $\mathbf{K}$ is the stiffness matrix in Voigt formulation. The symmetric matrix $\tilde{\mathbf{K}}$ can be shown to represent the components of a second-rank tensor in the 6D space [24]. In accordance with Ciampa and Meo [25], the aim of this approach consists of determining the eigenmoduli $\boldsymbol{\Lambda}$ and the associated eigentensors $\tilde{\boldsymbol{\varepsilon}}$ of Eq. (2) in order to form an ortho-normalized basis for the stress and strain tensors of the second rank. In this manner, these tensors can be decomposed with respect to this basis in the 6D space. In other words, we seek for the eigenvalues $\boldsymbol{\Lambda}$ (known as *Kelvin moduli*) that satisfy the following equation:

$$\left(\tilde{\mathbf{K}} - \boldsymbol{\Lambda}\mathbf{I}\right)\tilde{\boldsymbol{\varepsilon}} = 0. \tag{5}$$

Since the six-dimensional linear transformation $\tilde{\mathbf{K}}$ is assumed to be symmetric and positive definite, there will be a maximum of six positive eigenelastic constants Λ_i ($i = 1,\ldots,6$) associated to Eq. (5). In addition to the six values of $\boldsymbol{\Lambda}$, also six values of

$\widetilde{\boldsymbol{\varepsilon}}$ will be associated to the problem (5), which are denoted by the vector $\widetilde{\boldsymbol{\varepsilon}}^{(i)}$ in the 6D space. The stresses $\widetilde{\boldsymbol{\sigma}}^{(i)}$ obtained by multiplying $\widetilde{\boldsymbol{\varepsilon}}^{(i)}$ by the eigenvalues Λ_i are called the stress eigentensors. Therefore, a Cartesian basis in the 6D space can be constructed from the normalized strain eigentensors, denoted by $\widetilde{\mathbf{N}}$:

$$\widetilde{\boldsymbol{\varepsilon}} = \widetilde{\mathbf{N}}\left|\widetilde{\boldsymbol{\varepsilon}}\right|; \quad \left|\widetilde{\boldsymbol{\varepsilon}}\right|^2 = \widetilde{\boldsymbol{\varepsilon}} \cdot \widetilde{\boldsymbol{\varepsilon}}; \quad \widetilde{\mathbf{N}} \cdot \widetilde{\mathbf{N}} = 1. \tag{6}$$

Hence, the stress eigentensors can be written in terms of the normalized strain eigentensors using Eqs. (2), (5) and (6) as:

$$\widetilde{\boldsymbol{\sigma}}^{(i)} = \Lambda_i \widetilde{\boldsymbol{\varepsilon}}^{(i)}. \tag{7}$$

With respect to the 6D space, $\widetilde{\boldsymbol{\sigma}}$, $\widetilde{\boldsymbol{\varepsilon}}$ and $\widetilde{\mathbf{K}}$ have the following representation:

$$\begin{aligned} \widetilde{\boldsymbol{\sigma}} &= \sum_{i=1}^{6} \Lambda_i \widetilde{\boldsymbol{\varepsilon}}^{(i)} = \sum_{i=1}^{6} \Lambda_i \left|\widetilde{\boldsymbol{\varepsilon}}^{(i)}\right| \widetilde{\mathbf{N}}^{(i)} \\ \widetilde{\boldsymbol{\varepsilon}} &= \sum_{i=1}^{6} \widetilde{\boldsymbol{\varepsilon}}^{(i)} = \sum_{i=1}^{6} \left|\widetilde{\boldsymbol{\varepsilon}}^{(i)}\right| \widetilde{\mathbf{N}}^{(i)} \end{aligned} \tag{8}$$

and:

$$\widetilde{\mathbf{K}} = \sum_{i=1}^{6} \Lambda_i \widetilde{\mathbf{N}}^{(i)} \otimes \widetilde{\mathbf{N}}^{(i)} \tag{9}$$

where $\otimes$ indicated the tensor or dyadic product. The projection of the strain state given by Eq. (3) along the eigenvectors obtained using Eq. (8) defines the eigenstrain vector $\widetilde{\varepsilon}_i$. Thereby, the total elastic modulus due to nonlinear material behaviour defined in Eq. (1) becomes:

$$\widetilde{K}_{TOT,i} = \Lambda_i \left(1 + \beta \widetilde{\varepsilon}_i + \delta \widetilde{\varepsilon}_i^2 + \cdots\right). \tag{10}$$

Once the total elastic modulus $\widetilde{K}_{TOT,i}$ $(i = 1,\ldots,6)$ is obtained, according to Eqs. (10) and (9), the 6 x 6 nonlinear stiffness matrix $\mathbf{K}^{TOT}$ can be then transformed from Kelvin

to Voigt notation and it can be used for the implementation of the explicit FE numerical method at each individual time step.

2.1 Nonlinear Finite Element Simulation

The application of explicit FE analysis in wave propagation problems allows computing the nodal forces and displacements without recourse to a factorization of the global stiffness matrix in a step-by-step solution. Let us consider a 3D solid domain Ω with boundary Γ discretized with 3D elements. The weak form of the equilibrium equations for the continuum Ω can be derived from the displacement variational principle as follows [26]:

$$\mathbf{M}\ddot{\mathbf{u}} = \mathbf{F}^{ext} - \mathbf{F}^{\text{int}} \tag{11}$$

where the dots superscript denotes a second time derivative operation of the global displacement vector $\mathbf{u}$ and the external nodal forces vector $\mathbf{F}^{ext}$, the internal nodal forces vector $\mathbf{F}^{\text{int}}$ and the (lumped) diagonal mass matrix $\mathbf{M}$ are:

$$\mathbf{F}^{\text{int}} = \sum_{e=1}^{n_{el}} \mathbf{L}^{(e)T} \mathbf{C}^{(e)} \mathbf{L}^{(e)} \mathbf{u} \tag{12a}$$

$$\mathbf{F}^{ext} = \sum_{e=1}^{n_{el}} \mathbf{L}^{(e)T} \left[\int_{\Gamma^{(e)}} \mathbf{\Phi}^T \mathbf{t} d\Gamma + \int_{\Omega^{(e)}} \mathbf{\Phi}^T \mathbf{b}\, d\Omega \right] \tag{12b}$$

$$\mathbf{M} = \sum_{e=1}^{n_{el}} \mathbf{L}^{(e)T} \mathbf{m}^{(e)} \mathbf{L}^{(e)} \tag{12c}$$

where $\mathbf{L}^{(e)}$ is the Boolean connectivity matrix that gather the nodal displacement $\mathbf{d}^{(e)}$ of each element e to the global one over the entire domain Ω, n_{el} is the total number of elements, $\Omega^{(e)}$ and $\Gamma^{(e)}$ are the element domain and its boundary, $\mathbf{\Phi}^T$ is the transpose of the shape function matrix, $\mathbf{t}$ and $\mathbf{b}$ are the surface traction and body (inertial) force of

the element, respectively. The element stiffness matrix $\mathbf{C}^{(e)}$ in Eq. (12a) can be expressed in terms of the nonlinear stiffness matrix $\mathbf{K}^{TOT}$ as follows [27]:

$$\mathbf{C}^{(e)} = \int_{\Omega^{(e)}} \mathbf{B}^T \mathbf{K}^{TOT} \mathbf{B}\, d\Omega \tag{13}$$

whilst the element mass matrix in Eq. (12c) is:

$$\mathbf{m}^{(e)} = \int_{\Omega^{(e)}} \rho \mathbf{\Phi}^T \mathbf{\Phi} d\Omega\,. \tag{14}$$

Finally, the strain nodal displacement matrix is defined by:

$$\boldsymbol{\varepsilon} = \mathbf{B}\mathbf{L}^{(e)}\mathbf{u} \tag{15}$$

The global displacement at the instant of time k+1 using the central difference method is given by:

$$\mathbf{u}_{k+1} = \Delta t^2 \mathbf{M}^{-1}\left(\mathbf{F}_k^{ext} - \mathbf{F}_k^{\text{int}}\right) + 2\mathbf{u}_k - \mathbf{u}_{k-1}\,. \tag{16}$$

where k=0, 1, 2, … corresponds to times $t = 0$, $t = T$, $t = 2T$, …, and T is the time increment. To guarantee numerical stability to the method, the time increment used for the simulation satisfy the following condition [28]:

$$\begin{aligned} &T < T_{cr} \\ &T_{cr} = \frac{1}{\pi}\frac{1}{f_{\max}} \end{aligned} \tag{17}$$

where f_{max} is the largest natural frequency of the system. The numerical scheme defined by Eq. (16) can be used by those elements that present either linear or nonlinear features. Whilst in the former case, the nonlinear elastic moduli are zero, in the nonlinear case the nonlinear stiffness matrix of the element has to be constantly updated at each time step due to the amplitude dependence with the material constants.

3 Numerical Test Case

The influence of nonlinear material effects on the FE model illustrated above was first numerically verified on a 3D composite plate with dimensions 153 x 106 x 3 mm (Fig. 2).

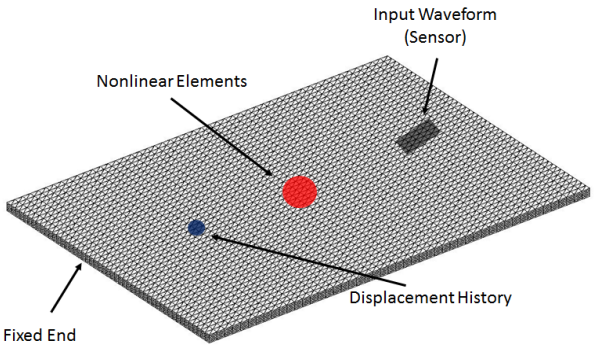

Figure 2 Geometry of the 3D composite plate.

The mesh was made of 15000 nodes with 77322 nodes in way that the element length was approximately 1 mm. The mechanical properties are reported in Table 1, whilst the stacking sequence for a quasi-isotropic laminate is $[0/45/90/-45]_s$.

Table 1: Orthotropic Material Properties

E_{11} (GPa)	E_{22} (GPa)	E_{33} (GPa)	G_{12} (GPa)	G_{23} (GPa)	G_{31} (GPa)	ν_{12}	ν_{23}	ν_{31}	ρ kg/m^3
131	9	9	5.7	5.37	5.37	0.3	0.29	0/34	1545

The numerical model was meshed with tetrahedral solid elements using the isoparametric formulation and it was implemented in an in-house FE code developed by the authors. According to Fig. 2, the plate was modelled in a cantilever position so that it was fixed at one end, whilst the other was kept free. The plate was dynamically

loaded with a continuous, harmonic and uniform in-plane traction force according to the following periodic law:

$$s(t) = A\sin(2\pi f_0 t) \tag{18}$$

where A is the amplitude of the input source and f_0 is the excitation frequency. In this case, an amplitude A=5x10^3 Pa and a fundamental frequency f_0=150 kHz were used. Such a time-dependent pressure distribution was applied from an area located at x_i=90 mm and y_i=48 mm on the top surface, in way to represent the numerical model of two sensors operating in pitch-catch mode. The output (in-plane displacement) of the numerical model was measured within a time window of $\tau = 5\times10^{-3}$ s and, according to Eq. (17), the sampling time (time step) was set to $T = 1\times10^{-7}$ s.

4 Experimental set-up

The experiments were carried out on a composite CFRP plate with the same dimensions and a lay-up sequence as in the numerical case (Fig. 3).

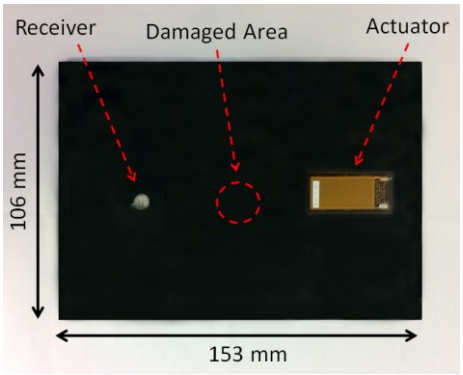

Figure 3 Experimental set-up.

A dropped-weight impact test machine with a hemispherical tip was used for hitting the test panel at 12 J. Such an energy level was chosen in order to inflict damage in the composite laminate corresponding to a BVID. In order to transmit the input source and

measure the material nonlinear response, two different surface bonded transducers were used, i.e. a broadband APC sensor with diameter of 6.35 mm and thickness of 2.55 mm, and a MFC-P2 transducer with length of 37 mm and width of 18 mm. The APC sensor was employed as receiver and it was instrumented with an oscilloscope (Picoscope 4224) with a sampling rate of 10 MHz and an acquisition window of $\tau = 5 \times 10^{-3}$ s. To transmit the continuous sinusoidal waveform with a frequency f_0=150 kHz, the MFC transducer was linked to a preamplifier and connected to an arbitrarily waveform generator (TTi-TGA12104). Additionally, the carbon fibre specimen was positioned on two foam pieces in order to reduce the environmental noise (Fig. 4).

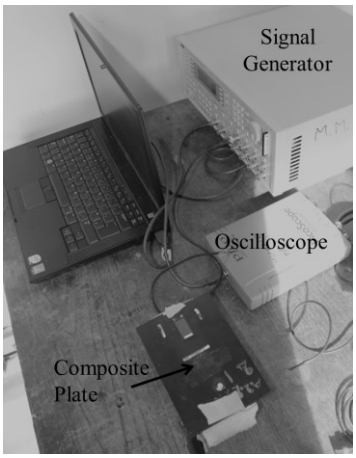

Figure 4 Set-up of the data acquisition system.

4.1 Evaluation of Damaged Area

In order to obtain a qualitative image of the delamination generated by the impact and, thus, to provide an indication of the damaged area, two standard NDT tests were performed, i.e. an ultrasonic C-Scan and an X-ray tomography (CT-Scan). In the first test, the "USL SCM 12X" ultrasonic C-Scan was used to image the defect (Fig. 5). Indeed, this linear ultrasonic test showed two damage locations with an "apparent" undamaged area in the middle of the composite specimen (represented by a white colour

area). However, since a protrusion occurred as a result of impact loading, the ultrasonic C-scan was able to reveal only the presence of damage within the laminate, but it was not able to detect and access the damaged area beneath this protrusion due to poor acoustic impedance.

Figure 5 Image of the defect using ultrasonic C-Scan.

Therefore, in way to obtain a quantitative estimation of the presence of delamination beneath the composite surface, a second nondestructive test was performed. In particular, a "Nikon Metrology XT H 225 ST" computational tomography machine was used to take a series of 2D X-ray images of the test specimen. Fig. 6 displays the damaged area at various depths caused by the impact within the cross-section of the material.

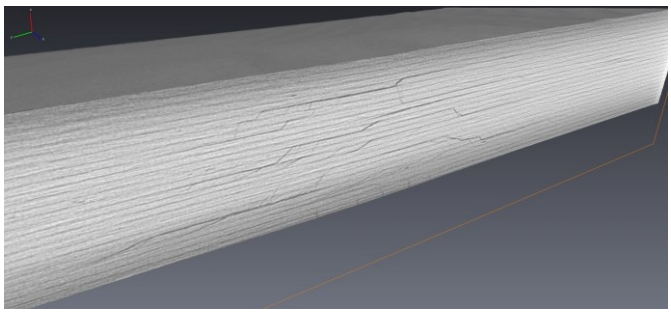

Figure 6 CT-scan image showing the damages occurred at a different depth.

Since at the impact point loaded laminates were pushed upwards causing all the laminates to move towards the top of the specimen, an indentation on the bottom and a protrusion on the top of the sample were generated. This resulted in the creation of a "pine tree" shape of the damage with three different delaminations occurred within the composite laminate (Fig. 6). Therefore, based on the CT-scan results, for the calculation of the damaged location a circular area was assumed with a radius of 10 mm and a thickness of 2 mm.

5 Numerical and Experimental Results

According to the previous section, the nonlinear classical material was modelled by imposing a combination of the semi-analytical Landau and Kelvin formulation to those elements within the damaged area. In this manner, the 3D nonlinear response to different types of stress waves could be simulated. In order to compare the amplitude of the second harmonic between the numerical model and the experimental test, only the influence of the second order nonlinear coefficient β was considered [Eq. (10)]. Moreover, the mesoscopic elements with nonlinear features were assumed to be uniformly distributed over a circular area with diameter of 20 mm and thickness of 2 mm located at the middle of the plate.

The quadratic nonlinear parameter β was experimentally calculated as the ratio between the amplitude of the second harmonic and the square value of the fundamental one, and it was used as an input for simulating the nonlinear behaviour of the composite structure. In our case a value of β=0.4 was found. Hence, the nonlinear signature (harmonic generation) could be easily disclosed by the analysis the recorded signals in the frequency domain. Fig. 7 shows the comparison of the fast Fourier transformation

(FFT) of the in-plane displacement component u_x at x_i=30 mm and y_i=50 mm from both the experimental and numerical (FE) tests.

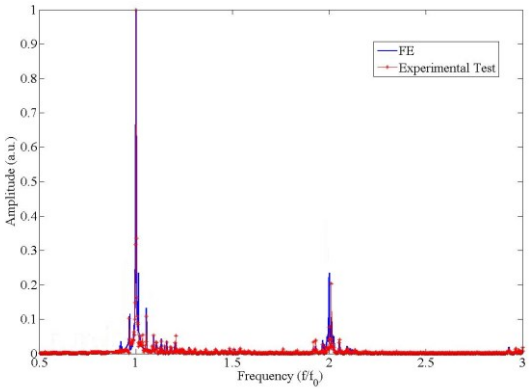

Figure 7 Comparison of the in-plane displacement spectra from experimental (red) and simulated (blue) material responses.

From Fig. 7 it can be clearly seen that a good agreement between the values of the second harmonic from the experimental and numerical tests was achieved. Indeed, in accordance with theoretical and experimental evidence [29], [30], [31], the second harmonic contribution is predominant in the measured material response due to the presence of damage. Moreover, it should be noted that the amplitude of the fundamental harmonic was normalized to a unit value. In this manner, it was possible to compare both simulated and experimental material responses in the case where no information about the mechanical pressure exerted by the actuator sensor was provided.

Hence, this numerical model can be employed to understand the nonlinear behaviour of 3D composite structure, or, alternatively, for nonlinear inverse problems, in which the size of the micro-crack or the fatigue crack grow can be estimated from the analysis of the harmonic structural responses.

Conclusions

The purpose of this study was to validate a numerical elastic material model with experimental results for the analysis of the nonlinear harmonic response in composite structures. By means of semi-analytical Landau and Kelvin formulation, this constitutive model allows the description of the structural response under continuous harmonic excitation in 3D composite laminates. In this manner, nonlinear elastic effects observed experimentally such as the second harmonic generation could be simulated. To validate the proposed model, experimental tests were conducted on a composite plate undergone to impact loading. Good agreement in the level magnitude of the second harmonic between the numerical and experimental tests, not only verify the validity of the theoretical model, but also shows its promising future in the application of nondestructive testing. Future work is now undergoing to extend this model to further nonlinear elastic phenomena such as vibro and inter-modulation (side-bands generation) in a variety of materials.

References

[1] J.-B Inh, F.-K Chang. Pitch-catch active sensing method in structural health monitoring for aircraft structures. *Struct Health Monit* **7**(1), 5-19 (2008).

[2] V. Giurgiutiu, A. Zagrai, J.-J. Bao. Piezoelectric waver embedded active sensors for aging aircraft structural health monitoring. *Struct Health Monit* **1**(1), 41-61 (2002).

[3] W. J.-N. de Lima and M.-F. Hamilton, "Finite-amplitude waves in isotropic elastic plates", J. Sound Vib. **265**, 819 (2003).

[4] K. E.-A. Van Den Abeele, K. Van de Velde, J. Carmeliet. “Inferring the degradation of pultruded composites from dynamic nonlinear resonance measurements”, Polym. Compos. **22**, 555-567, (2001).

[5] P.-B. Nagy, L. Adler. “Acoustic Nonlinearity in plastics”, in Review of Progress in Quantitative Nondestructive Evaluation, edited by D. O. Thompson and D. E. Chimenti (Plenum, New York, 1992), Vol. **I IB**, 2025-2032, (1992).

[6] C. Pecorari. “Nonlinear interaction of plane ultrasonic waves with an interface between rough surfaces in contact”. *J. Acoust. Soc. Am*. ***113*** (*6*), 3065-72 (2003).

[7] J.H.-Cantrell. “Fundamentals and applications of non-linear ultrasonic non-destructive evaluation”. In: Kundu Tribikiram, editor. Ultrasonic non-destructive evaluation, vol. 6. Boca Raton (FL): CRC Press; 363-434 (2004)

[8] K. E.-A. Van Den Abeele, P.-A. Johnston, A. Sutin. “Nonlinear elastic wave spectroscopy (NEWS) techniques to discern material damage, part I: nonlinear wave modulation spectroscopy (NWMS)”. *Res. Nondestr. Eval.* ***12*** (*1*), 17-30 (2000).

[9] F. Ciampa, M. Meo. “Nonlinear elastic imaging using reciprocal time reversal and third order symmetry analysis”. *J. Acoust. Soc. Am*. ***131*** (*6*), pp. 4316-23 (2012)

[10] V.-V. Kazakov, A. Sutin, and P.-A. Johnson. “Sensitive imaging of an elastic nonlinear wave-scattering source in a solid”, *Appl. Phys. Lett.* ***81***, 646–648 (2002)

[11] O. Bou Matar, P.-Y Guerder, Y. Li, B. Vandewoestyne, K. E.-A. Van Den Abeele. “A nodal discontinuous Galerkin finite element method for nonlinear elastic wave propagation”. *J. Acoust. Soc. Am*. ***131*** (*5*), pp. 3650-63 (2012)

[12] S. Hirose, J.-D. Achenback, “Higher harmonics in the far field due to dynamic crack-face contacting”, *J. Acoust. Soc. Am.,* **93** (1), pp. 142–147 (1993)

[13] P. Delsanto, M. Scalerandi, “A spring model for the simulation of the propagation of ultrasonic pulses through imperfect contact interfaces”, J. *Acoust. Soc. Am*., **104**, 2584 (1998)

[14] M. Scalerandi, V. Agostini, P.-P Delsanto, K. E.-A. Van Den Abeele, P.-A. Johnson. “Local interaction simulation approach to modelling nonclassical, nonlinear elastic behaviour in solids”. *J. Acoust. Soc. Am*. ***113*** (*6*), (2003).

[15] K. E.-A. Van Den Abeele, F. Shubert, V. Aleshin, F. Windels. J. Carmeliet. “Resonnat bar simulations in media with localized damage”, Ultrasonics **42** (1-9), 1017-1024 (2004).

[16] S. Vanaverbeke, K. E.-A. Van Den Abeele. “Two-dimensional modelling of wave propagation in materials with hysteretic nonlinearity”, *J. Acoust. Soc. Am.*, **122**, pp. 58–72 (2007).

[17] G. Zumpano, M. Meo. “A new nonlinear elastic time reversal acoustic method for the identification and localisation of stress corrosion cracking in welded plate-like structures – A simulation study”. *Int. J. Solids Struct.* ***44***, 3666–84 (2007).

[18] E. Barbieri, M. Meo. “Time reversal DORT method applied to nonlinear elastic wave scattering”. *Wave Motion* ***47*** *(7)*, 452–467 (2010).

[19] L. Ostrovsky, P.-A. Johnson. “Dynamic nonlinear elasticity in geomaterials”. *Riv. Nuovo Cim.* ***24***, 1−46 (2001).

[20] P.-A. Johnson. The Universality of Nonclassical Nonlinearity (with application to Nondestructive Evaluation and Ultrasonics), Chap. 4, Springer New York, 49–69, (2006).

[21] L.-D. Landau, E.-M. Lifshitz, Theory of Elasticity, Pergamon, Oxford, (1986).

[22] G. Zumpano, M. Meo. “A new damage detection technique based on wave propagation for rails”. *Int. J. Solids Struct.* ***43*** (5), 1023–46 (2006).

[23] K. Helbig and P. N.-J Rasolofosaon. “A theoretical paradigm for describing hysteresis and nonlinear elasticity in arbitrary anisotropic rocks” in *Proceedings of the Ninth International Workshop on Seismic Anisotropy*, Society of Exploration Geopysicistry, Tulsa, (2000).

[24] P.-S. Theocaris, D.-P. Sokolis. “Spectral decomposition of the compliance fourth-rank tensor for orthotropic materials” *Archive of Applied Mechanics*, **70**: 289-306, (2000).

[25] F. Ciampa, E. Barbieri, M. Meo. “Modelling of Multiscale Nonlinear Interaction of Elastic Waves with 3D Cracks”. Manuscript submitted to *Journal of Acoustical Society of America* (2013)

[26] K.-J. Bathe. Finite Element Procedures in Engineering Analysis. Prentice-Hall Inc., (1982).

[27] R.-D. Cook, D.-S. Malkus, M.-E. Plesha. Concepts and applications of finite element analysis, third ed. John Wiley & Sons, (1989).

[28] J. Donea. Advanced Structural Dynamics, Applied Science Publishers, Barking. Essex (1980).

[29] M. Meo, G. Zumpano. “Nonlinear elastic wave spectroscopy identification of impact damage on sandwich plate”. *Compos Struct **71***, 469–474 (2005).

[30] G. Zumpano, M. Meo. “Damage localization using transient non-linear elastic wave spectroscopy on composite structures”. *Int. J. Nonlin. Mech.* **43**, 217-230, (2008).

[31] K. E.-A. Van Den Abeele, A. Sutin, J. Carmeliet, P. A. Johnston. “Micro-damage diagnostics using nonlinear elastic wave spectroscopy (NEWS)”. *NDT&E International, Vol. **34***, 239-248 (2001)